ACS Catalysis

Research Article

pubs.acs.org/acscatalysis

Correlating Heat of Adsorption of CO to Reaction Selectivity: Geometric Effects vs Electronic Effects in Neopentane Isomerization over Pt and Pd Catalysts

David Childers,[†] Arindom Saha,[‡] Neil Schweitzer,[§] Robert M. Rioux,[‡] Jeffrey T. Miller,[§] and Randall J. Meyer*,[†]

[†]Department of Chemical Engineering, University of Illinois at Chicago, Chicago, Illinois 60607, United States

[‡]Department of Chemical Engineering, The Pennsylvania State University, University Park, Pennsylvania 16802, United States

[§]Division of Chemical Sciences and Engineering, Argonne National Laboratory, 9700 S. Cass Avenue, Lemont, Illinois 60439, United States

Supporting Information

ABSTRACT: Silica-supported Pt and Pd nanoparticles from 1 to 10 nm in diameter were evaluated for neopentane conversion (hydrogenolysis and isomerization). Characterization of the catalysts was conducted utilizing scanning transmission electron microscopy (STEM), diffuse reflectance infrared Fourier transform spectroscopy (DRIFTS) of adsorbed CO, X-ray absorption spectroscopy (XAS), and isothermal calorimetry of CO adsorption to determine how geometric or electronic structure effects can explain changes in reactivity. Isomerization selectivity of Pt was much higher than Pd for all particle sizes. There is a pronounced effect of particle size on selectivity, with the highest isomerization selectivity achieved over catalysts containing the largest particle size for both Pt (57%) and Pd (26%) catalysts. For both Pd and Pt catalysts, DRIFTS showed a decrease in the ratio of linear-to-bridge bonded CO with particle size, while isothermal calorimetry of CO adsorption shows that both Pt and Pd enthalpies of adsorption decrease with increasing particle size. The isomerization selectivity was found to correlate inversely with the strength of CO adsorption for all catalysts suggesting that the chemisorption energy and not the particle size, coordination geometry, or ensemble size is the most important factor for increasing the isomerization selectivity.

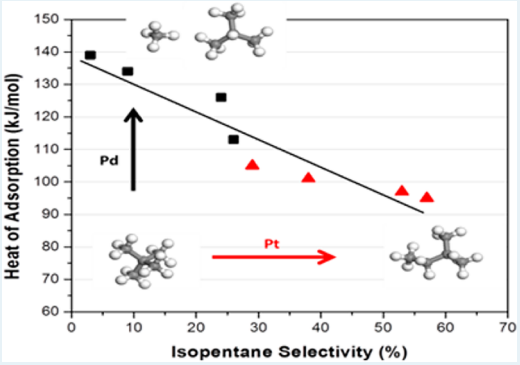

KEYWORDS: *particle size effects, neopentane, hydrogenolysis, isomerization, calorimetry*

1. INTRODUCTION

The demand for fossil fuels will continue to grow as demand for mobile energy sources increases rapidly in emerging markets. Therefore, advances in naphtha reforming processes will remain an important area for the foreseeable future.[1] Aside from increased demand, stricter regulations will require refining processes to adjust in response to mandated higher quality standards. Selective isomerization and aromatization of alkanes (inclusive of normal and branched hydrocarbons) is an important process to improve the quality of transportation fuels. Cracking or hydrogenolysis reactions occur in parallel with isomerization; therefore, minimizing selectivity to hydrogenolysis products is an important quality of improved catalysts for this class of reactions.

Catalytic naphtha reforming is a major reaction in petroleum refining which involves the conversion of straight-chain *n*-alkanes to branched alkanes, the dehydrogenation of cycloalkanes, and the dehydrogenation and cyclization of alkanes to aromatics.[2] The main purpose of naphtha reforming is to increase the octane number of a naphtha feedstock for the production of gasoline. The primary components of typical catalysts for hydrocarbon reforming are late d-band transition metals such as Pt; while commercial catalysts are often complex alloys composed of late d-band transition metals and selectivity promoting metals such as Sn and Re. The study of real naphtha reforming on a laboratory scale is difficult because of the number of products and the experimental difficulties associated with multiphase systems. Therefore, the conversion of neopentane was investigated to gain a general understanding of how paraffins undergo ring closure or hydrogenolysis to undesirable light gas products.[2,3]

Neopentane hydrogenolysis has been widely used as a model reaction for the characterization of noble metal catalysts.[4−10] Neopentane conversion has two possible reaction pathways as shown in Figure 1.[3,11,12]

Received: July 8, 2013
Revised: September 18, 2013
Published: September 20, 2013

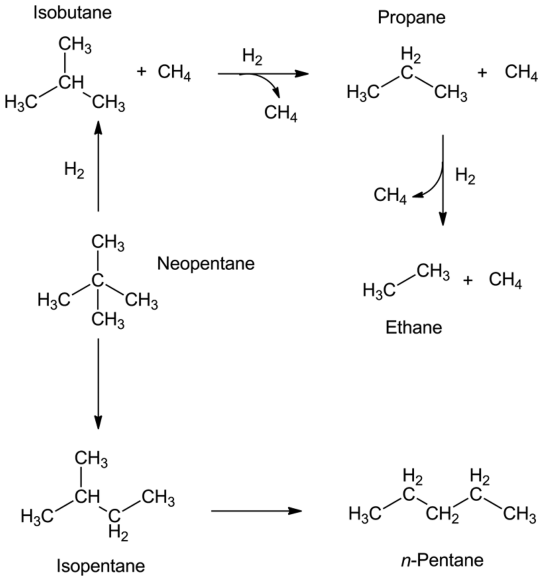

Figure 1. Reaction pathways for neopentane conversion. The two pathways, isomerization and hydrogenolysis, occur both in parallel and in series. Isomerization products can undergo hydrogenolysis after isomerization.

As illustrated in Figure 1, the primary products include methane and iso-butane for hydrogenolysis and isopentane for isomerization. In both cases, further reaction can occur to produce secondary products, such as propane and additional methane. Each hydrogenolysis step produces one mole of methane per mole of *n*-alkane. Further isomerization of the primary isomerization product, isopentane, can lead to formation of *n*-pentane. Isomerization involves ring closure-ring-opening through a cyclopropyl intermediate to produce isopentane.[5] The selectivity for ring closure in naphtha reforming is important for the production of aromatics from paraffins, while hydrogenolysis leads to liquid yield loss.[1,3,13] Properties leading to higher isomerization selectivity for neopentane to isopentane, generally lead to higher aromatic selectivity for naphtha reforming catalysts.

Neopentane (also known as 2,2-dimethylpropane) cannot form olefins or carbenium ions prior to isomerization which occasionally are observed as deleterious side reactions occurring over the metal oxide catalyst support in hydrocarbon reforming processes.[8,9] Only metal-catalyzed reactions are possible and selectivity studies are much easier to perform. In addition, neopentane hydrogenolysis and isomerization is a popular test reaction because of minimal catalyst deactivation.[4]

Neopentane reforming has been studied on both supported Pt and Pd catalysts.[6−9,14,15] Karpinski and Juszczyk examined Pd/SiO_2 and found a maximum isomerization selectivity of 30% for severely sintered (30−50 nm) Pd particles.[14] This reaction was also conducted over Pd/Al_2O_3 catalysts, and a maximum isomerization selectivity of 25% was observed.[7] Boudart et al. studied a series of transition metals (Pt, Os, Ir, Au, Ru, Rh, and Pd) for neopentane reforming and found that only 5d metals, such as Ir, Pt, and Au isomerized neopentane to isopentane.[5] They determined the selectivity and activity depended on the nanoparticle structure (the presence of a single type of site or an ensemble of sites) and that there were two possible configurations for neopentane to adsorb onto platinum: a η^3-adsorbed (three bonds to the surface) and η^2-adsorbed (two bonds to the surface) intermediate with a lower rate of hydrogenolysis for the η^3-adsorbed intermediate. Their results supported a mechanism previously proposed by Anderson and Avery, in which the adsorbed hydrocarbon is [(1,3-η)neopentane]platinum with one sp^2 carbon forming a double bond with a surface atom, from which isomerization occurs through a ring closure−ring-opening mechanism on the surface.[15] This mechanism requires a minimum of two surface sites to bind a neopentane molecule.[5]

Foger et al. performed a particle size study of Pt on silica to confirm the mechanism proposed earlier by Anderson and Avery.[6] At the largest size studied, around 20 nm, the isomerization selectivity was about 70%. They found the isomerization selectivity increased with particle size from 1 to 20 nm (0 to 70%). This change in selectivity was attributed to the relative increase in the proportion of Pt surface atoms composing (111) terraces. On the low surface energy (111) surface, the isomerization pathway dominates. They also proposed the hydrogenolysis pathway only needs a single Pt site (in contrast to previous results) and that lower coordinated Pt atoms would be the favored site for this reaction.[5,6,16,17] Smaller particle sizes will have a greater proportion of these lower coordination sites on the surface compared to larger particles. Ponec et al. conducted a particle size study (1 to 14 nm range) on Pt using 2,2-dimethylbutane as the probe molecule, which also has isomerization and hydrogenolysis pathways, and found that there was an increase in isomerization selectivity with increasing particle size.[10]

In this study we confirmed the Pt particle size study done by Foger et al. and used various characterization techniques to determine the importance of geometric and electronic effects on neopentane conversion and selectivity. By keeping the support the same for all catalysts as well as the reaction conditions, the effect of particle size was isolated. In addition, we compared the activity and selectivity results for neopentane hydrogenolysis to CO adsorption by infrared spectroscopy and also calorimetry, to determine the properties of the catalyst which are most influential in controlling selectivity to hydrogenolysis versus isomerization products.

2. EXPERIMENTAL METHODS

2.1. Synthesis of Platinum and Palladium Catalysts. Platinum and palladium samples were synthesized on a silica (Davisil A60) support. Incipient wetness impregnation (IWI) and strong electrostatic adsorption (SEA) were the two methods used.[18] IWI is the most widely used industry technique and also the simplest. During IWI, a support is contacted with just enough metal-precursor solution to fill the pore volume. All of the metal precursor solution contacts the surface because of the incipient amount of liquid used; however, there can be significant particle growth during drying and pretreatment. In contrast, SEA uses excess solution with a controlled pH to favor uptake of the metal precursor. The use of excess solution does not necessitate that all of the metal precursor will adsorb to the surface of the catalyst support. The SEA method requires an appropriately charged metal precursor based on the point of zero charge (PZC) of an oxide support and the pH of the solution. The hydroxyl groups on the surface of the oxide support will protonate or deprotonate depending on the pH of the solution relative to the PZC of the support. Precursors can then be selected that have the opposite overall charge as the support at a certain pH value; the electrostatic interaction between the support and the precursor leads to strong binding of the metal precursor to the surface. This

dx.doi.org/10.1021/cs400527p | *ACS Catal.* 2013, 3, 2487−2496

Table 1. Catalyst Precursors and Treatment Steps

sample	synthesis method	precursor	calcination temperature (°C)	reduction temperature (°C)
3%Pd/SiO_2_1 nm	SEA (pH = 11)	$Pd(NH_3)_4NO_3$	125	165
2%Pd/SiO_2_2.5 nm	IWI	$Pd(NH_3)_4NO_3$	125	225
2%Pd/SiO_2_3 nm	IWI	$Pd(NO_3)_2$	225	225
2%Pd/SiO_2_8.1 nm	IWI	$Pd(NO_3)_2$	300	225
1%Pt/SiO_2_1.2 nm	SEA (pH = 11)	$Pt(NH_3)_4(NO_3)_2$	125	300
1%Pt/SiO_2_1.5 nm	SEA (pH = 11)	$Pt(NH_3)_4(NO_3)_2$	300	300
1%Pt/SiO_2_6.6 nm	SEA (pH = 11)	$Pt(NH_3)_4(NO_3)_2$	425	300
1%Pt/SiO_2_10 nm	SEA (pH = 11)	$Pt(NH_3)_4(NO_3)_2$	525	300

allows for strong monolayer adsorption and can reduce sintering during the post-treatment steps.[18]

For the Pd catalysts, both $Pd(NO_3)_2$ and $Pd(NH_3)_4(NO_3)_2$ were used as precursors. IWI was the method of synthesis for catalysts with medium to large size particles while SEA (at a pH = 11 with NH_4OH) was used to obtain a catalyst with small particles. Samples were calcined and reduced at different temperatures to influence the final particle size. The Pt samples were made by the SEA (at a pH = 11 with NH_4OH) method in one large batch using $Pt(NH_3)_4(NO_3)_2$ as the precursor. For the Pt catalysts, we varied the calcination temperature from no calcination to 525 °C to synthesize catalysts with various particle sizes. Catalyst reduction was accomplished in a 4% H_2/He mixture at the final temperature for 1 h. Synthesis method and treatment steps are given in Table 1.

2.2. Scanning Transmission Electron Microscopy (STEM). STEM images were obtained at UIC's Research Resources Center facility using the JEOL-ARM 200CF aberration corrected microscope (70 pm spatial resolution and 300 meV energy resolution). Samples were dispersed in isopropyl alcohol and sonicated for 20 min. A drop of the suspension was added dropwise to a holey-carbon copper grid and dried under a heat lamp for 20 min. Images were taken using the High Angle Angular Dark Field (HAADF) mode and particle size was counted using the Particule2 program. A minimum of 100 particles were counted to get an accurate representation of the particle size distribution for each catalyst.

2.3. Extended X-ray Absorption Fine-Structure Spectroscopy (EXAFS). X-ray absorption spectroscopy (XAS) measurements at the Pd K (24350 eV), and Pt L_3 (11564 eV) edges were made on the bending magnet beamline of the Materials Research Collaborative Access Team (MRCAT) at the Advanced Photon Source (APS), Argonne National Laboratory. Measurements were made in transmission mode. A platinum or palladium foil spectrum was acquired through a third ion chamber simultaneously with each measurement for energy calibration.

Samples were prepared by grinding the catalysts into a fine powder and pressing them into the sample holder. The sample holder is a metal cylinder capable of holding up to six individual samples. The sample holder is then placed in a quartz tube with ports on each end to flow gases or isolate the sample after treatment. The sample thickness was chosen to give a total absorbance at the Pt L_3 or Pd K edge between 1 and 2 absorption lengths and edge steps around 0.3−0.5. Samples were reduced at 250 °C in a 4% H_2/He mixture (50 cm^3/min) at atmospheric pressure. After reduction, the samples were purged with He at 100 cm^3/min and cooled to room temperature in He flow. Trace oxidants in He were removed by a Matheson PUR-Gas Triple Purifier Cartridge containing a Cu trap. All EXAFS spectra were obtained at room temperature in He.

2.4. Neopentane Hydrogenolysis and Isomerization. Neopentane hydrogenolysis and isomerization was studied using 0.05−0.15 g of catalyst diluted with 0.9 g of silica and loaded into a 0.5" OD quartz plug flow reactor. Glass wool was used for the bottom 2 cm of the bed. A 0.5 cm silica layer was placed on top of the glass wool before the catalyst and silica mixture was added to the reactor resulting in a catalyst bed height of 3 cm. The reactor was purged with He for 5 min before each run, and the catalyst was reduced in 4% H_2/He as the temperature was increased to the reaction temperature, 271 ± 2 °C. This temperature enabled differential (conversion) operation for all of the catalysts tested. A K-type thermocouple was inserted from the bottom of the reactor into the lower portion of the catalyst bed. Once the reaction temperature stabilized, the pre-mixed reactant feed gas consisting of 0.35% neopentane and 3.5% H_2 balanced in He was passed through the reactor. The flow rate of the feed gas was varied from 25 to 100 cm^3/min to obtain differential conversion (0.5−6%). Each flow rate was run for at least 1 h to ensure steady-state conversion had been reached. An Agilent 6890N gas chromatograph with an FID detector was used to analyze the products. The GC column (a J&W Scientific GS-Alumina column) was equipped with a back pressure regulator to hold the system at a constant pressure of 9 psig. Each experimental run was completed within 6 h for consistency, and multiple runs for each catalyst were performed. No appreciable deactivation was observed in any of the catalysts over this period of time. The maximum error of any selectivity measurements was 6%, with most of the data being reproducible within 2%. Turnover rates were calculated based upon the number of active sites determined by the dispersion measured by STEM (the dispersion was estimated to be 1/particle diameter (nm)). Using the EXAFS data or CO chemisorption determined dispersion data to determine the number of active sites gave only slight differences with regard to the turnover frequency values and does not alter any of the conclusions reached below.

2.5. Diffuse Reflectance Infrared Fourier Transform Spectroscopy (DRIFTS). Infrared spectra were obtained with an ABB Laboratory FTLA2000 FTIR spectrometer. Samples were ground to a very fine powder using a mortar and pestle, and packed into the sample chamber to create the most uniform surface possible. The chamber was purged with He, and then the gas was switched to H_2 and the temperature was raised to 250 °C and held for 15 min. After reduction of the catalyst, the gas was switched back to He, and the temperature was reduced to 25 °C. A background scan was then recorded, which was averaged over at least 256 scans with 4 cm^{-1} resolution. The sample was then exposed to 1.6% CO/N_2 for 20 min to saturate the sample. The flow was then changed back

dx.doi.org/10.1021/cs400527p | ACS Catal. 2013, 3, 2487−2496

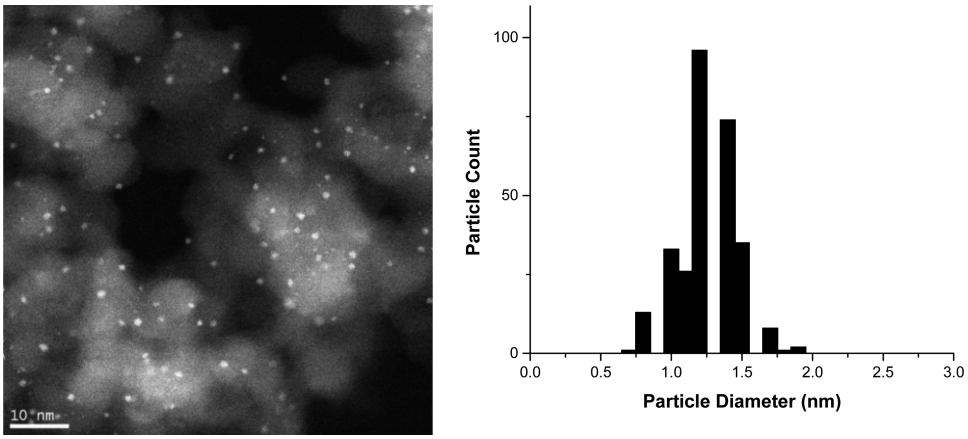

Figure 2. 1% Pt/SiO_2_1.2 nm sample image and particle size distribution determined by STEM.

to He, and a final set of scans were taken once the intensity of the adsorbed CO peaks were invariant with time, which took anywhere from 2 to 6 h depending on the catalyst. Linear to Bridging ratios were taken from the integrated intensities of the absorption spectra without further correction. It should be noted that the sensitivity of the intensity to linear CO and bridging CO vary due to variations in the strength of the dipole in the C−O bond on different sites. Therefore the L:B ratios should be taken as a qualitative measure of the relative populations only.[19−22]

2.6. CO Heats of Adsorption. The heat of adsorption measurements for CO adsorption on the Pd and Pt catalysts were carried out using a volumetric adsorption apparatus (Micromeritics ASAP 2020C) that has been interfaced with a differential scanning calorimeter (Setaram Sensys EVO differential scanning calorimeter (DSC)). Pd catalysts were re-reduced at 200 °C in pure H_2 for 1 h, subsequently purged with He that had been passed through an Oxytrap at 200 °C for 1 h prior to cooling to the adsorption temperature (35 °C). The Pt catalysts were subjected to a similar treatment sequence, except that the pre-reduced catalysts were re-reduced at 275 °C for 1 h in pure H_2 and purged with oxygen-free He for 1 h at the same temperature before cooling to the adsorption temperature (35 °C).

The combined volumetric adsorption−calorimetry experiments were designed so that a significant number of low pressure data points were collected to measure the differential heat of adsorption at low coverage. Heat flow due to adsorption is measured simultaneously with measurement of adsorption uptake, such that a differential heat of adsorption, $\Delta H(\theta)$ can be determined by dividing the measured heat flow by the amount adsorbed determined by the Micromeritics adsorption apparatus. The uncertainty for these measurements are given as ±5 kJ/mol due to instrument error based on the standard deviation of repeat analysis (N = 5) on one of the supported Pd/SiO_2 catalysts.

3. RESULTS AND DISCUSSION

3.1. Particle Size Analysis. Particle size was determined using STEM imaging. A STEM image for the 1% Pt/SiO_2_1.2 nm sample and the corresponding size distribution are shown in Figure 2; the average particle size is 1.2 nm. The STEM particle size of the Pt and Pd catalysts are summarized in Table 2 and Supporting Information, Figure S1.

Table 2. Particle Sizes Determined by STEM, EXAFS, and CO Chemisorption

sample	particle size by STEM (nm)	particle size by EXAFS (nm)	particle size by CO_{irr} chemisorption (nm)[a,b]
3%Pd/SiO_2_1 nm	1.0 ± 0.2	1.0 ± 0.1	1.7 ± 0.2
2%Pd/SiO_2_2.5 nm	2.5 ± 1.1	2.5 ± 0.3	4.3 ± 0.4
2%Pd/SiO_2_3 nm	3.0 ± 0.8	5.0 ± 0.5	3.8 ± 0.4
2%Pd/SiO_2_8.1 nm	8.1 ± 1.7	10 ± 1.0	9.9 ± 1.0
1%Pt/SiO_2_1.2 nm	1.2 ± 0.2	1.1 ± 0.1	1.5 ± 0.2
1%Pt/SiO_2_1.5 nm	1.5 ± 0.8	1.5 ± 0.2	1.3 ± 0.1
1%Pt/SiO_2_6.6 nm	6.6 ± 2.6	5.0 ± 0.5	5.8 ± 0.6
1%Pt/SiO_2_10 nm	10 ± 5.2	8.0 ± 0.8	8.3 ± 0.8

[a]Monolayer uptake (extrapolated to P = 0) at 35 °C using the dual isotherm technique assuming a CO:Pd_s (or Pt_s) stoichiometry of unity. [b]Based on d (nm) = c/D, where c is constant and equal to 0.994 for Pd and D is the dispersion, or ratio of the number of surface atoms to the total number of atoms in the catalyst sample.

EXAFS spectroscopy was also used to evaluate particle size using the K edge of Pd and L_3 edge of Pt. The EXAFS component of the data was fit to obtain a coordination number and an interatomic distance (See Supporting Information, Table S1). The coordination number, N, is used to estimate the particle size based on a hemispherical geometry and the lattice constant derived according to the equation:[23]

$$\log\left(\frac{\mathrm{H}}{\mathrm{Pt}}\right) = -0.132 \times (N_{\mathrm{Pt-Pt}}) + 2.58$$

This equation has been checked against STEM and other size data and is applicable to Pd by adjusting the parameters by 0.5% to account for the difference in lattice constants. Table 2 shows the results of the STEM, EXAFS, and chemisorption particle size analysis; the results demonstrate generally good agreement between the three techniques. All three techniques indicate the average particle size of Pt and Pd varies between 1 and 10 nm.

3.2. Reactivity Results. Figure 3 shows the effect of conversion on selectivity (under differential conversion) for the 1%Pt/SiO_2_1.2 nm catalyst. Product selectivity was plotted, and the selectivity extrapolated to 0% conversion; these numbers are reported in Table 3 along with the calculated turnover rate (TOR). The turnover rates presented are based on the molecules of neopentane converted per surface atom and so activity has been normalized per surface atom. Products

dx.doi.org/10.1021/cs400527p | ACS Catal. 2013, 3, 2487−2496

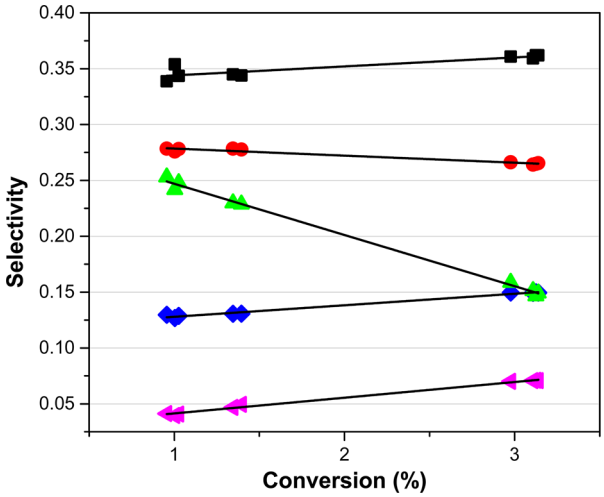

Figure 3. Selectivity for the 1% Pt(1.2 nm)_SiO_2 catalyst at differential conversion. Reaction conditions were 0.35% neopentane, 3.5% H_2, balance He, and 271 °C. The straight lines are included as a guide. Methane (black squares), ethane (red circles), propane (pink side triangles), isobutane (blue diamonds), and isopentane (green triangles).

with nonzero selectivity at 0% conversion are considered primary products while products that have 0% selectivity at 0% conversion are considered secondary products. For both Pd and Pt, the amount of methane produced decreases as the particle size increases, suggesting selectivity for hydrogenolysis decreases with increasing particle size.

However, the data in Table 3 also suggests the simple reaction scheme in Figure 1 may not be completely accurate since propane and ethane are observed at zero conversion. For example, in Figure 3 (1% Pt/SiO_2_1.2 nm), the initial selectivity to both ethane (11%) and propane (2%) are nonzero. This implies multiple surface reactions occur on the small Pd and all Pt catalysts before products desorb. On the Pt catalysts with ∼1−2 nm particle size, the high ethane selectivity implies there is an initial isomerization to a chemisorbed isopentyl intermediate followed by selective hydrogenolysis to give ethane, but little propane. This suggests the propyl fragment is strongly bound to the surface and undergoes further reaction to ethane and methane. Unlike small Pt nanoparticles, for 1 nm Pd the selectivity to propane (13%) is greater than ethane (1%), suggesting that after the initial hydrogenolysis reaction there is a second hydrogenolysis of the isobutyl surface intermediate. Davis et al. examined the conversion of neopentane over Pt single crystal surfaces and found that the (100) and (13,1,1) surfaces produced significantly more ethane and propane than the (111), (10,8,7), and (332) surfaces. The formation of these products was attributed to a skeletal isomerization step preceding hydrogenolysis.[24] Similarly, the presence of *n*-pentane in the limit of zero conversion over large Pt nanoparticles indicates that adsorbed neopentane can also undergo two isomerization steps before desorbing. Davis et al. found significant *n*-pentane production (12−14%) on the (100) and (13,1,1) surfaces and attributed the high selectivity to *n*-pentane to two rearrangements occurring during a single adsorption to the surface.[24] In our previous study of neopentane hydrogenolysis over Pt, Pd, and PdPt bimetallic catalysts, *n*-pentane formed over the monometallic Pt and the bimetallic catalysts with a particle size of ∼1−2 nm.[25]

Figure 4 shows both the Pt and the Pd particle size effect on selectivity to isopentane, the primary product of the isomerization pathway. The selectivity to isopentane over Pt catalysts is in good agreement with the previous work of Foger et al. over a comparable particle size range. Pd catalysts exhibit the same trend although the selectivity to isopentane is ∼30% lower than the selectivity of a Pt catalyst with the same particle size. The isomerization selectivity (only 3%) was very low for the smallest Pd particles but increased to a maximum of 26% for the largest particle size (8 nm). The smallest Pt particles had a higher selectivity to isopentane (29%) than the largest Pd (26%), but both metals exhibited a similar trend: isomerization selectivity increased with increasing particle size. This result seems to support Anderson and Avery's mechanism which

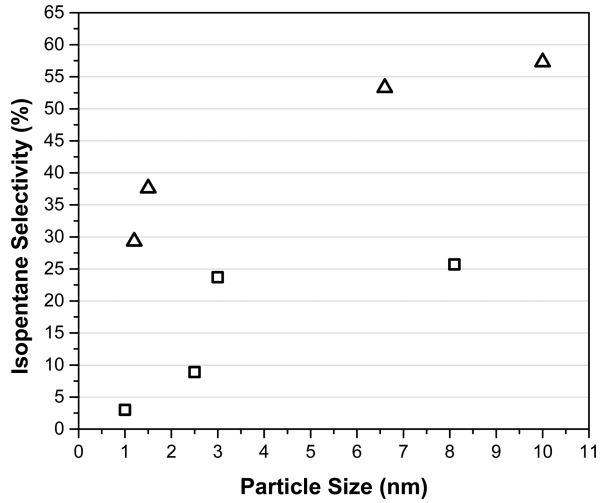

Figure 4. Isopentane selectivity as a function of particle size for silica-supported Pd (□) and Pt (Δ). Reaction conditions were 0.35% neopentane, 3.5% H_2, balance He, and 271 °C.

Table 3. TOR and Product Selectivity for the Pt and Pd Catalysts

			initial product distribution (%)						
catalyst	dispersion (by STEM)	TOR	CH_4	C_2H_6	C_3H_8	*n*-C_4H_{10}	*i*-C_4H_{10}	*i*-C_5H_{12}	*n*-C_5H_{12}
3%Pd/SiO_2_1 nm	1.0	1.0×10^{-3}	55	1	13	0	28	3	0
2%Pd/SiO_2_2.5 nm	0.40	1.0×10^{-3}	49	1	5	2	33	9	0
2%Pd/SiO_2_3 nm	0.33	7.7×10^{-4}	40	0	1	1	34	24	0
2%Pd/SiO_2_8.1 nm	0.12	1.1×10^{-3}	39	1	2	1	32	26	0
1%Pt/SiO_2_1.2 nm	0.83	1.4×10^{-3}	33	11	2	0	28	29	0
1%Pt/SiO_2_1.5 nm	0.67	1.0×10^{-3}	29	6	2	0	25	38	0
1%Pt/SiO_2_6.6 nm	0.15	8.0×10^{-4}	23	3	2	0	20	53	6
1%Pt/SiO_2_10 nm	0.10	2.3×10^{-4}	19	2	2	0	16	57	5

dx.doi.org/10.1021/cs400527p | *ACS Catal.* 2013, 3, 2487−2496

postulates the η^3-adsorbed state is the necessary surface intermediate for isomerization and therefore it could be expected that larger (111) surface facets promote isomerization selectivity.[5] As the particle size increases there will be a greater fraction of low energy (111) surface sites as opposed to smaller particles which will contain more corners and edges that disfavor adsorption of neopentane in the η^3-adsorbed state. Conversely, edges and corners are known to favor C−H and C−C bond cleavage, required events for hydrogenolysis.[26] While this model suggests selectivity is related to the presence (or absence) of particular sites on the surface and can explain the selectivity trend for a single metal, it does not account for the changes in absolute selectivity values between metals (i.e., Pt > Pd by about 30%).

Figure 5 demonstrates the TOR of Pd catalysts (square) for neopentane conversion varies little with particle size, while the

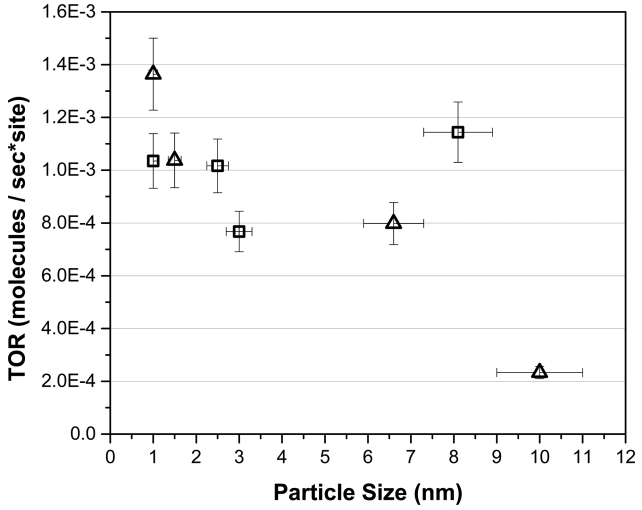

Figure 5. Overall TOR for Pd (□) and Pt (Δ) catalysts. Reaction conditions were 0.35% neopentane, 3.5% H_2, balance He, and 271 °C.

Pt catalysts (triangle) display a steady decrease in activity with increasing particle size.

The turnover rates for isomerization and hydrogenolysis for Pd catalysts are shown in Figure 6. For Pd, the TOR for hydrogenolysis (circle) is invariant or decreases slightly with increasing particle size, similar to the trend for the overall TOR. However, the isomerization TOR appears to increase with increasing particle size. The increase in the TOR for isomerization correlates with the increase in the surface area of the (111) faces. However, the magnitude of the isomerization TOR is not very significant compared to the TOR for hydrogenolysis, so any trend for isomerization is obscured by the variance in the measured hydrogenolysis rate.

Figure 7 shows the isomerization (square) and hydrogenolysis (circle) TORs for the Pt catalysts. In contrast to Pd, there is a decrease in hydrogenolysis TOR with increasing particle size, similar to the decrease in overall TOR shown in Figure 5B. In addition, the isomerization TOR does not follow the same trend as found for Pd. From the data, one cannot conclude there is an increase in the isomerization TOR with increasing size. For both metals, the hydrogenolysis TOR mirrors the overall TOR.

3.3. Diffuse Reflectance Infrared Fourier Transform Spectroscopy (DRIFTS). Figure 8 shows the compiled DRIFTS spectra of adsorbed CO on the Pd catalysts. For the

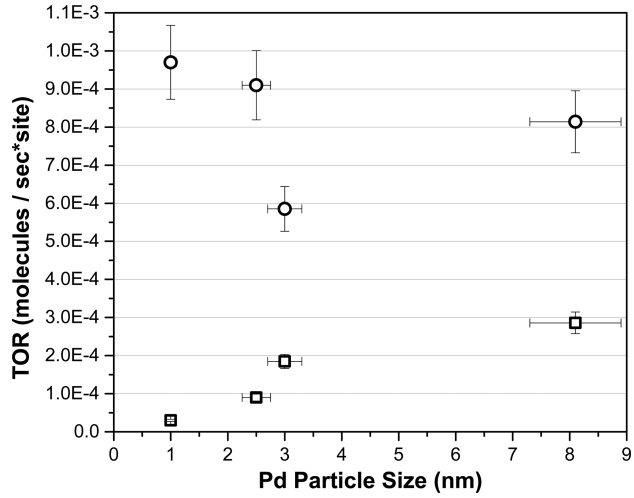

Figure 6. Isomerization (□) and hydrogenolysis (○) TOR for silica-supported Pd catalysts. Reaction conditions were 0.35% neopentane, 3.5% H_2, balance He, and 271 °C.

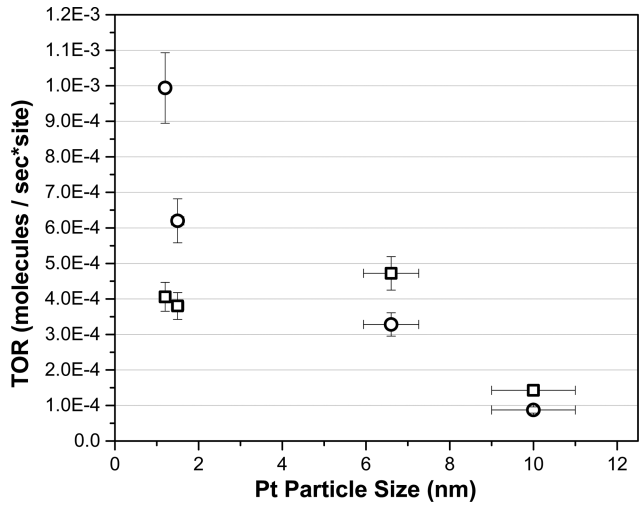

Figure 7. Isomerization (□) and hydrogenolysis (○) TOR for silica-supported Pt catalysts. Reaction conditions were 0.35% neopentane, 3.5% H_2, balance He, and 271 °C.

catalyst with the smallest Pd particle size, there is a large absorbance around 2090 cm^{-1} which is attributed to linear bound CO, and another peak at ∼1950 cm^{-1} assigned to bridge-bonded CO.[27−29] As the particle size increases there is a sharp decrease in the linearly adsorbed CO (∼2090 cm^{-1}). The absorbance of the bridge-bonded CO peak (∼1950 cm^{-1}) decreases with particle size, but the overall linear-to-bridging ratio still decreases with increasing particle size (Table 4). At larger Pd sizes (>1 nm), the bridge-bonded CO peak at ∼1950 cm^{-1} splits into two distinct peaks. These two peaks can be attributed to bridge-bonded CO on terraces and bridge-bonded CO on corner and edge sites.[30,31] These results are consistent with an increasing ratio of large, flat surfaces (represented by bridge-bonded CO) as particle size increases. These results are consistent with those by Bradley et al.[29]

Figure 9 shows the DRIFTS spectra for adsorption of carbon monoxide on the silica-supported Pt catalysts. There is a very sharp peak at ∼2050 cm^{-1}, which is assigned to linear-bonded CO, and a much smaller and broader peak centered at ∼1800 cm^{-1}, assigned to bridge-bonded CO.[32−37] Similar to the Pd

dx.doi.org/10.1021/cs400527p | ACS Catal. 2013, 3, 2487−2496

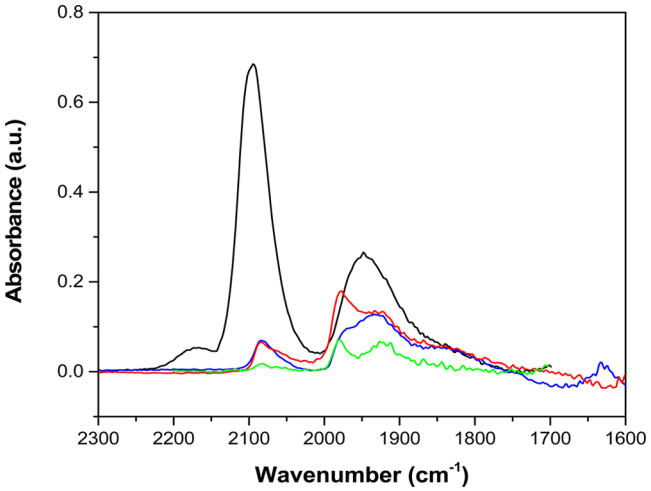

Figure 8. DRIFTS spectra of the adsorption of carbon monoxide on silica-supported Pd catalysts at room temperature. 1.0 nm (black line), 2.5 nm (blue line), 3.0 nm (red line), and 8.1 nm (green line).

Table 4. Particle Size Dependent CO Initial Heat of Adsorption Values (±5 kJ/mol) and Linear to Bridging Ratio for CO at Saturation Coverage

sample	initial CO heat of adsorption (kJ mol^{-1})	linear-to-bridging ratio
3Pd_1.0 nm	139	1.5:1
2Pd_2.5 nm	134	0.19:1
2Pd_3.0 nm	126	0.20:1
2Pd_8.1 nm	113	0.14:1
1Pt_1.2 nm	105	3.5:1
1Pt_1.5 nm	101	3.0:1
1Pt_6.6 nm	97	2.3:1
1Pt_10.0 nm	95	1.3:1

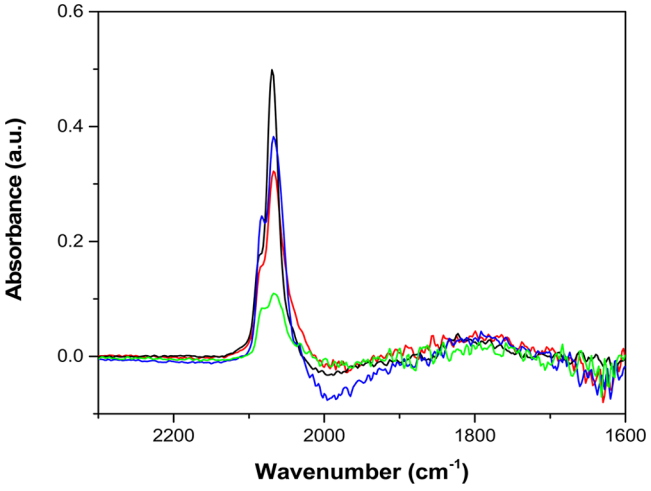

Figure 9. DRIFTS spectra of the adsorption of carbon monoxide on silica-supported Pt catalysts at room temperature. 1.2 nm (black line), 1.5 nm (blue line), 6.6 nm (red line), and 10 nm (green line).

samples, there is a dramatic decrease in the absorbance of the linear-bonded CO adsorption peak with increasing particle size while the bridge-bonded CO peak shows a smaller decrease in absorbance over the particle size range examined. Similar to Pd, the linear-to-bridge bonded CO absorbance ratio decreases with increasing particle size. A similar trend emerges for both the Pt and the Pd catalysts, although the linear peak for the Pt samples remains more prominent than Pd at the larger particle sizes. These results for Pt are also consistent with those by Singh et al. and Bradley et al.[34,36] The linear-to-bridged bonded ratios (determined by area) for both Pt and Pd samples are given in Table 4.

3.4. Heat of Adsorption of CO Determined by Isothermal Calorimetry. Just as in the case of the DRIFTS experiments mentioned in the previous section, we have used CO as a probe molecule to examine how the heat of adsorption may relate to the activity and selectivity for neopentane conversion. Since neopentane adsorbs weakly at 35 °C (Kao et al. reported that neopentane desorbs from both Pt and Pd (111) surfaces at 200 K) we have chosen to use CO as a surrogate molecule.[38,39] There is ample literature data on the heat of adsorption of CO on both Pt and Pd for comparison with the values determined in this work.[40−52] The enthalpies of CO adsorption for Pt and Pd nanoparticles of different size are given in Table 4. The initial heats of adsorption of the Pd samples are similar to those reported in the literature.[53−55] Chou et al. performed a heat of adsorption study on Pd particles of various sizes supported on silica; the values reported by Chou et al. are similar to the values reported in Table 4. Sen et al. performed a study of CO heat of adsorption on Pt/SiO_2 catalysts of different sizes and determined little to no size effect though the values obtained are similar to the ones reported here.[42] This conclusion was based mainly on the fact that the change was not as drastic as the one found for Pd; however their data does show a decreasing trend. For both Pt and Pd nanoparticles, the enthalpy of CO adsorption decreases with increasing particle size, although the relationship is more pronounced for the Pd samples.

Now that we have established a relationship between particle size and heat of adsorption in a similar fashion to the previous observation of selectivity trends with particle size, a correlation may be made between the heat of adsorption of CO and isomerization selectivity. Figure 10 demonstrates that for both Pt and Pd catalysts there is a single correlation between the initial heat of CO adsorption and the neopentane isomerization selectivity, and that the lower the heat of adsorption, the higher the isomerization selectivity. It should be noted that this

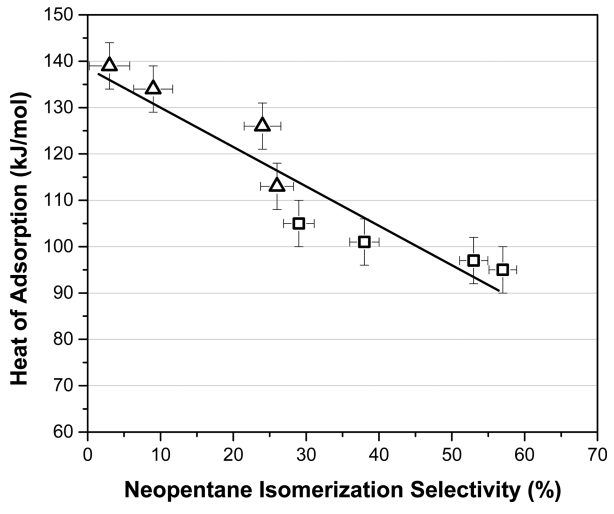

Figure 10. Isomerization selectivity versus CO heat of adsorption for Pd (triangles) and Pt (squares) catalysts.

dx.doi.org/10.1021/cs400527p | ACS Catal. 2013, 3, 2487−2496

relationship between the initial heat of adsorption of CO and the isomerization activity is independent of the type of adsorption site as the binding site for CO clearly changes (as seen in the IR experiments and reported in Table 4) as a function of particle size. In addition, the isomerization selectivity and enthalpy of adsorption of the 8 nm Pd (26% and 113 kJ/mol) and 1.2 nm Pt (29% and 105 kJ/mol) nanoparticles are very similar suggesting that the chemisorption energy and not the particle size, coordination geometry, or ensemble size is the important factor for increasing the isomerization selectivity. Previous models suggest that large (111) surfaces are essential for high isomerization selectivity, but the smallest Pt nanoparticles (1.2 nm) are shown to have almost identical selectivity to the largest Pd nanoparticles (8.1 nm). This implies the mechanisms for both isomerization and hydrogenolysis are invariant at low-coordinate and high-coordinate sites or that the structure of the site is not the most relevant property of the catalyst. This idea is supported by Davis et al. who performed neopentane conversion over Pt single crystal surfaces and found that there was little influence of surface structure on the rate and selectivity of the reaction.[24,56] Given this strong correlation between selectivity and CO heats of adsorption, it would appear that the strength of the metal-adsorbate bond is the dominating factor for tuning selectivity.

Previously, Norskov and co-workers have shown that simple descriptors such as the oxygen binding energy can be used to predict reactivity.[57] In addition, it has been found that there is a linear relationship between the location of the d-band center and the adsorption energy of simple adsorbates. For example, Liu and Norskov demonstrated a linear relationship to describe the correlation between the d-band center of Pd surfaces and the adsorption energy of CO.[58,59] Similarly, Nakamura and co-workers developed a linear correlation between the binding energy of a methyl fragment and the d-band center.[60]

Expanding this idea in their study of acetylene hydrogenation, Studt et al. used the heat of adsorption of a methyl group as a simple descriptor which is correlated with the heat of adsorption of acetylene, and therefore a descriptor of acetylene hydrogenation for a large variety of metal surfaces (including Pd and Pd alloys).[61] Just as in the case of correlating the adsorption of one hydrocarbon to another, we suggest here that since both hydrocarbon adsorption and CO adsorption are linear functions of the d-band center, then a relationship must exist between CO adsorption and hydrocarbon adsorption. In fact, using the two sets of data correlating the d-band center with the adsorption energies of CO and CH_3, one can combine these two relationships to establish a linear correlation between the adsorption energy of CO and the adsorption energy of CH_3:[59,60]

$$E_{CO,ads} = 0.60E_{CH3,ads} - 0.09 \quad \text{(energies in eV)}$$

Therefore since a linear relationship between hydrocarbon adsorption and CO adsorption seems evident, the linear relationship in Figure 10 implies that the adsorption energy of neopentane is a critical factor in determining selectivity. However, since relatively little is known about neopentane adsorption on metal surfaces, CO chemisorption serves as a more general predictor of isomerization selectivity. Correlating selectivity with heat of adsorption has been demonstrated by Studt et al. in the hydrogenation of acetylene to ethylene. While the activity decreased as a function of decreasing adsorption energy of acetylene, the selectivity increased as the adsorption energy decreased. In this work, the selectivity similarly increases as the adsorption energy decreases. However, it is not clear why the activity does not exhibit a similar response as function of the adsorption energy.

We can test this correlation by examining literature data for various metals. For example, rhodium is known to perform hydrogenolysis almost exclusively and has an initial CO heat of adsorption around 140 kJ/mol which agrees with the correlation in Figure 10.[62,63] Iridium is shown to have some isomerization selectivity (~7%) for *n*-butane reactions and an initial CO heat of adsorption of around 146 kJ/mol.[64,65] Although this is a slightly different reaction and the Ir was supported on alumina rather than silica, this data still falls within our correlation. Therefore, if this correlation is true, the value for the CO heat of adsorption should be predictive for improving the isomerization selectivity of supported catalysts. Pt alloyed with Sn is widely used in industry to improve the selectivity of Pt catalysts.[49,66] Shen et al. performed CO adsorption experiments on Pt and PtSn alloys and found a decrease of nearly 20 kJ/mol upon the addition of Sn. Schwank et al. found isopentane selectivities of 75−80% on Pt−Sn alloys supported on alumina.[4] From reported values of CO heats of adsorption of various bimetallics it should be possible to predict the neopentane isomerization selectivity. Ultimately, the correlation that we observe between the CO adsorption energy and the isomerization selectivity provides a simple method for predicting catalysts which may exhibit even higher selectivity than reported here. Further work on specific bimetallic samples will be used test this relation between selectivity and bond strength and determine how far one may extend this correlation.

4. CONCLUSION

Both Pt and Pd exhibit a clear particle size effect in terms of neopentane isomerization selectivity. Both metals display increasing isomerization selectivity with increasing particle size with Pt having a significantly higher selectivity than Pd at an equivalent particle size. While such a trend might suggest this change in selectivity results from a geometric effect, the correlation between the isomerization selectivity and the initial heat of adsorption of CO suggests isomerization and hydrogenolysis selectivity are determined by the strength of the metal adsorbate bond independent of the particle size, coordination geometry of the surface atoms, or the type of metal. This result implies that the observed selectivity for isomerization is primarily a function of electronic effects (i.e., the strength of the bond between the metal surface and the adsorbate) and is not a strong function of the coordination of the adsorbate to the surface. In addition, for all catalysts, at very low conversion there are reaction products that indicate multiple surface reactions before desorption. These consecutive reactions were especially important for nanoparticles of less than 2 nm in size where the enthalpies of adsorption were largest.

■ ASSOCIATED CONTENT

Ⓢ Supporting Information

STEM images and particle size distributions. This material is available free of charge via the Internet at http://pubs.acs.org.

■ AUTHOR INFORMATION

Corresponding Author

*E-mail: rjm@uic.edu.

Notes

The authors declare no competing financial interest.

■ ACKNOWLEDGMENTS

J.T.M. and N.S. were supported as part of the Institute for Atom-Efficient Chemical Transformations (IACT), an Energy Frontier Research Center funded by the U.S. Department of Energy, Office of Science, Office of Basic Energy Sciences. R.J.M. and D.C. gratefully acknowledge funding for this work from the National Science Foundation (CBET Grant 0747646). Partial funding for D.C. was provided by the Chemical Sciences and Engineering Division at Argonne National Laboratory and the Office of the Vice Chancellor for Research at the University of Illinois at Chicago. The STEM work was performed at the UIC Research Resource Center. R.M.R. acknowledges financial support provided through a 3M Non-Tenured Faculty Grant (NTFG). Use of the Advanced Photon Source was supported by the U.S. Department of Energy, Office of Science, Office of Basic Energy Sciences, under Contract No. DE-AC02-06CH11357. MRCAT operations are supported by the Department of Energy and the MRCAT member institutions.

■ REFERENCES

(1) Akhmedov, V. M.; a. A.-K., S. H. *Catal. Rev. - Sci. Eng.* **2007**, *49* (1), 33−139.
(2) Antos, G. J., Aitani, A. M., Eds.; *Catalytic Naphtha Reforming*, 2nd ed.; Marcel Dekker, Inc.: New York, 2004; p 602.
(3) Antos, G. J., Aitani, A. M., Parera, J. M., Eds.; Reforming Processes. In *Catalytic Naphtha Reforming*, 1st ed.; Marcel Dekker, Inc.: New York, 1995; p 415.
(4) Balakrishnan, K.; Schwank, J. *J. Catal.* **1991**, *132* (2), 451−464.
(5) Boudart, M.; Ptak, L. D. *J. Catal.* **1970**, *16* (1), 90.
(6) Foger, K.; Anderson, J. R. *J. Catal.* **1978**, *54* (3), 318−335.
(7) Juszczyk, W.; Lomot, D.; Karpinski, Z.; Pielaszek, J. *Catal. Lett.* **1995**, *31* (1), 37−45.
(8) Juszczyk, W.; Karpinski, Z. *J. Catal.* **1989**, *117* (2), 519−532.
(9) Juszczyk, W.; Karpinski, Z.; Ratajczykowa, I.; Stanasiuk, Z.; Zielinski, J.; Sheu, L. L.; Sachtler, W. M. H. *J. Catal.* **1989**, *120* (1), 68−77.
(10) Botman, M. J. P.; Devreugd, K.; Zandbergen, H. W.; Deblock, R.; Ponec, V. *J. Catal.* **1989**, *116* (2), 467−479.
(11) Akhmedov, V. M.; Al-Khowaiter, S. H. *Catal. Rev.* **2007**, *49* (1), 33−139.
(12) Ciapetta, F. G.; Wallace, D. N. *Catal. Rev.* **1972**, *5* (1), 67−158.
(13) Ciapetta, F. G.; Wallace, D. N. *Catal. Rev.* **1972**, *5* (1), 67−158.
(14) Karpinski, Z.; Juszczyk, W.; Pielaszek, J. *J. Chem. Soc., Faraday Trans. I* **1987**, *83*, 1293−1305.
(15) Anderson, J. R.; Avery, N. R. *J. Catal.* **1966**, *5*, 446−463.
(16) Cortright, R. D.; Watwe, R. M.; Spiewak, B. E.; Dumesic, J. A. *Catal. Today* **1999**, *53* (3), 395−406.
(17) Cremer, P.; Stanners, C.; Niemantsverdriet, J. W.; Shen, Y. R.; Somorjai, G. *Surf. Sci.* **1995**, *328* (1−2), 111−118.
(18) *Catalyst Preparation: Science and Engineering*; Regalbuto, J. R., Ed.; CRC Press: Boca Raton, FL, 2006; p 488.
(19) Schweizer, E.; Persson, B. N. J.; Tushaus, M.; Hoge, D.; Bradshaw, A. M. *Surf. Sci.* **1989**, *213*, 49−89.
(20) Hoffmann, F. *Surf. Sci. Rep.* **1983**, *3* (2−3), 109−192.
(21) Vannice, M. A.; Twu, C. C. *J. Chem. Phys.* **1981**, *75* (12), 5944−5948.
(22) Vannice, M. A.; Wang, S.-Y. *J. Phys. Chem.* **1981**, *85* (17), 2543−2546.
(23) Miller, J. T.; Kropf, A. J.; Zha, Y.; Regalbuto, J. R.; Delannoy, L.; Louis, C.; Bus, E.; van Bokhoven, J. A. *J. Catal.* **2006**, *240* (2), 222−234.
(24) Davis, S. M.; Zaera, F.; Somorjai, G. A. *J. Am. Chem. Soc.* **1982**, *104* (26), 7453−7461.
(25) Wu, T. P.; Childers, D. J.; Gomez, C.; Karim, A. M.; Schweitzer, N. M.; Kropf, A. J.; Wang, H.; Bolin, T. B.; Hu, Y. F.; Kovarik, L.; Meyer, R. J.; Miller, J. T. *ACS Catal.* **2012**, *2* (11), 2433−2443.
(26) Egeberg, R. C.; Larsen, J. H.; Chorkendorff, I. *Phys. Chem. Chem. Phys.* **2001**, *3* (11), 2007−2011.
(27) Giorgi, J. B.; Schroeder, T.; Baumer, M.; Freund, H. J. *Surf. Sci.* **2002**, *498* (1−2), L71−L77.
(28) Rebelli, J.; Rodriguez, A. A.; Ma, S. G.; Williams, C. T.; Monnier, J. R. *Catal. Today* **2011**, *160* (1), 170−178.
(29) Bradley, J. S.; Hill, E. W.; Behal, S.; Klein, C.; Chaudret, B.; Duteil, A. *Chem. Mater.* **1992**, *4* (6), 1234−1239.
(30) Lear, T. K.; Thomas; Baumer, M.; Rupprechter, G.; Freund, H.-J.; Lennon, D. *J. Chem. Phys.* **2005**, *123*, 13.
(31) Lu, J. F.; Baosong; Kung, M. C.; Xiao, G.; Elam, J.; Kung, H. H.; Stair, P. C. *Science* **2012**, *335*, 4.
(32) Haaland, D. M. *Surf. Sci.* **1987**, *185* (1−2), 1−14.
(33) Balakrishnan, K.; Sachdev, A.; Schwank, L. *J. Catal.* **1990**, *121* (2), 441−455.
(34) Singh, J.; van Bokhoven, J. A. *Catal. Today* **2010**, *155* (3−4), 199−205.
(35) Veldurthi, S.; Shin, C. H.; Joo, O. S.; Jung, K. D. *Catal. Today* **2012**, *185* (1), 88−93.
(36) Bradley, J. S.; Millar, J. M.; Hill, E. W.; Behal, S. *J. Catal.* **1991**, *129* (2), 530−539.
(37) Bradshaw, A. M. *Surf. Sci.* **1985**, *158* (1−3), 624−627.
(38) Kao, C. L.; Madix, R. J. *J. Phys. Chem. B* **2002**, *106* (33), 8248−8257.
(39) Street, K. L.; Fiorin, V.; McCoustra, M. R. S.; Chesters, M. A. *Surf. Sci.* **1999**, *433*, 176−179.
(40) Chou, P.; Vannice, M. A. *J. Catal.* **1987**, *104* (1), 17−30.
(41) Sen, B.; Vannice, M. A. *J. Catal.* **1991**, *130* (1), 9−20.
(42) Sen, B.; Vannice, M. A. *J. Catal.* **1991**, *130* (1), 9−20.
(43) Vannice, M. A.; Chou, P. *ACS Symp. Ser.* **1986**, *298*, 76−88.
(44) Vannice, M. A.; Hasselbring, L. C.; Sen, B. *J. Catal.* **1986**, *97* (1), 66−74.
(45) Vannice, M. A.; Hasselbring, L. C.; Sen, B. *J. Catal.* **1985**, *95* (1), 57−70.
(46) Vannice, M. A.; Hasselbring, L. C.; Sen, B. *J. Phys. Chem.* **1985**, *89* (14), 2972−2973.
(47) Vannice, M. A.; Sen, B.; Chou, P. *Rev. Sci. Instrum.* **1987**, *58* (4), 647−653.
(48) Hill, J. M.; Shen, J. Y.; Watwe, R. M.; Dumesic, J. A. *Langmuir* **2000**, *16* (5), 2213−2219.
(49) Shen, J. Y.; Hill, J. M.; Watwe, R. M.; Spiewak, B. E.; Dumesic, J. A. *J. Phys. Chem. B* **1999**, *103* (19), 3923−3934.
(50) Sharma, S. B.; Ouraipyvan, P.; Nair, H. A.; Balaraman, P.; Root, T. W.; Dumesic, J. A. *J. Catal.* **1994**, *150* (2), 234−242.
(51) Silvestre, J.; Sanchez-Castillo, M.; He, R.; Rodriguez-Reinoso, F.; Dumesic, J. A. *Catal. Lett.* **2002**, *82* (1−2), 153−153.
(52) Silvestre-Albero, J.; Sanchez-Castillo, M. A.; He, R.; Sepulveda-Escribano, A.; Rodriguez-Reinoso, F.; Dumesic, J. A. *Catal. Lett.* **2001**, *74* (1−2), 17−25.
(53) Li, M. S.; Shen, J. Y. *Mater. Chem. Phys.* **2001**, *68* (1−3), 204−209.
(54) Gravellerumeaumaillot, M.; Pitchon, V.; Martin, G. A.; Praliaud, H. *Appl. Catal., A* **1993**, *98* (1), 45−59.
(55) Chou, P.; Vannice, M. A. *J. Catal.* **1987**, *104* (1), 17−30.
(56) Davis, S. M.; Gillespie, W. D.; Somorjai, G. A. *J. Catal.* **1983**, *83* (1), 131−140.
(57) Greeley, J.; Norskov, J. K. *Surf. Sci.* **2005**, *592* (1−3), 104−111.
(58) Liu, P.; Norskov, J. K. *Phys. Chem. Chem. Phys.* **2001**, *3* (17), 3814−3818.
(59) Hammer, B.; Morikawa, Y.; Norskov, J. K. *Phys. Rev. Lett.* **1996**, *76* (12), 2141−2144.
(60) Wang, G. C.; Li, J.; Xu, X. F.; Li, R. F.; Nakamura, J. *J. Comput. Chem.* **2005**, *26* (9), 871−878.

(61) Studt, F.; Abild-Pedersen, F.; Bligaard, T.; Sorensen, R. Z.; Christensen, C. H.; Norskov, J. K. *Science* **2008**, *320* (5881), 1320−1322.
(62) Wong, T. T. T.; Sachtler, W. M. H. *J. Catal.* **1993**, *141* (2), 407−418.
(63) He, R.; Kusaka, H.; Mavrikakis, M.; Dumesic, J. A. *J. Catal.* **2003**, *217* (1), 209−221.
(64) Bourane, A.; Nawdali, M.; Bianchi, D. *J. Phys. Chem. B* **2002**, *106* (10), 2665−2671.
(65) Bond, G. C.; Yahya, R. *J. Chem. Soc., Faraday Trans.* **1991**, *87* (5), 775−781.
(66) Cortright, R. D.; Levin, P. E.; Dumesic, J. A. *Ind. Eng. Chem. Res.* **1998**, *37* (5), 1717−1723.